

Analyst

Accepted Manuscript



This is an *Accepted Manuscript*, which has been through the Royal Society of Chemistry peer review process and has been accepted for publication.

Accepted Manuscripts are published online shortly after acceptance, before technical editing, formatting and proof reading. Using this free service, authors can make their results available to the community, in citable form, before we publish the edited article. We will replace this *Accepted Manuscript* with the edited and formatted *Advance Article* as soon as it is available.

You can find more information about *Accepted Manuscripts* in the [Information for Authors](#).

Please note that technical editing may introduce minor changes to the text and/or graphics, which may alter content. The journal's standard [Terms & Conditions](#) and the [Ethical guidelines](#) still apply. In no event shall the Royal Society of Chemistry be held responsible for any errors or omissions in this *Accepted Manuscript* or any consequences arising from the use of any information it contains.

1
2
3
4
5
6
7
8
9
10
11
12
13
14
15
16
17
18
19
20
21
22
23
24

Modeling Vapor Uptake Induced Mobility Shifts in Peptide Ions Observed with Transversal Modulation Ion Mobility Spectrometry-Mass Spectrometry

25 Vivek K. Rawat¹, Guillermo Vidal-de-Miguel^{2,3} and Christopher J. Hogan Jr.*¹

26
27
28 ¹Department of Mechanical Engineering, University of Minnesota, Minneapolis, MN, USA

29 ² SEADM, Boecillo, Valladolid, Spain

30 ³Department of Chemistry and Applied Biosciences, ETH Zurich, Zürich, Switzerland.
31
32
33
34
35
36
37
38
39
40
41
42
43
44
45
46
47
48
49
50
51
52
53
54

Submitted to:

Analyst

55 *To whom correspondence should be addressed: hogan108@umn.edu, Tel: 1-612-626-
56 8312, Fax: 1-612-625-6069
57
58
59
60

ABSTRACT

Low field ion mobility spectrometry-mass spectrometry (IMS-MS) techniques exhibit low orthogonality, as inverse mobility often scales with mass to charge ratio. This inadequacy can be mitigated by adding vapor dopants, which may cluster with analyte ions and shift their mobilities by amounts independent of both mass and mobility of the ion. It is therefore important to understand the interactions of vapor dopants with ions, to better quantify the extent of dopant facilitated mobility shifts. Here, we develop predictive models of vapor dopant facilitated mobility shifts, and compare model calculations to measurements of mobility shifts for peptide ions exposed to variable gas phase concentrations of isopropanol. Mobility measurements were made at atmospheric pressure and room temperature using a recently developed transversal modulation ion mobility spectrometer (TMIMS). Results are compared to three separate models, wherein mobility shifts due to vapor dopants are attributed to changes in gas composition and (I) no vapor dopant uptake is assumed, (II) site-specific dopant uptake by the ion is assumed (approximated via a Langmuir adsorption model), and (III) site-unspecific dopant uptake by the ion is assumed (approximated via a classical nucleation model). We find that mobility shifts in peptide ions are in excellent agreement with model II, site-specific binding predictions. Conversely, mobility shifts of tetraalkylammonium ions from previous measurements were compared with these models and best agreement was found with model III predictions, i.e. site-unspecific dopant uptake.

1. INTRODUCTION

Although low field ion mobility spectrometry-mass spectrometry (IMS-MS) can be used for two-dimensional separation and analysis of complex analyte mixtures (such as peptide mixtures^{1, 2}), an ion's inverse mobility tends to scale with its mass-to-charge ratio³⁻⁶, and IMS-MS separations are relatively low in orthogonality relative to other two-dimensional separation techniques (e.g. LC-MS^{7, 8}). In fact, for many analytes within the same structural family, it is possible to develop correlation curves linking mobility directly to mass^{6, 9-13}. For this reason, low field IMS-MS separations can require the use of IMS instruments with extremely high resolving power (in excess of 50) relative to their high field or non-linear mobility counterparts (e.g. FAIMS^{14, 15}) in order to resolve small differences in mobilities between structural isomers. A potential method to mitigate such high resolving power requirements is through the addition of vapor phase dopants in ion mobility instruments, such as water, acetone, or alcohols; these species can cluster with analyte ions selectively, shifting their mobility by an analyte dependent amount¹⁶⁻¹⁸. As this shift typically does not necessarily scale with ion mass or mobility, the introduction of vapor dopants can appreciably increase the orthogonality of IMS-MS separation, hence vapor dopants have been used in IMS-MS analysis of peptide ions⁹, carbohydrate precursor ions¹⁹ and explosives/chemical warfare agent detection.²⁰⁻²²

However, while applications vapor dopant induced mobility shifts in IMS separations have been presented previously, little effort has been devoted to quantification of the extent of mobility shifts. Quantification of mobility shifts, performed by linking measured mobilities to models of ion interaction with vapor dopants, would serve to aid in designing vapor dopant uptake IMS-MS separation schemes; presently, vapor dopant concentrations are selected by trial-and-error approaches with little consideration of the expected shift in mobility²³. In addition, by

1
2
3 linking measurements to models of mobility shifts, which are based on specific vapor molecule
4 uptake mechanisms, information on the nature of interaction (e.g. site-specific binding versus
5 non-specific adsorption) between dopant molecules and analyte ions can be gained.
6
7
8
9

10 Along these lines, in this study we develop models to quantify mobility shifts for ions in
11 the presence of vapor dopants. As a test system, we used a recently developed transversal
12 modulation ion mobility spectrometer (TMIMS)²⁴⁻²⁶ coupled to a mass spectrometer to make
13 measurements of 5 ions in a standard peptide mixture. Ions were produced via electrospray
14 ionization and controlled amounts of isopropanol were introduced into the TMIMS cell,
15 facilitating isopropanol uptake by peptide ions. Results are compared and contrasted with recent
16 measurements of mobility induced shifts for tetraalkylammonium ions made with the same
17 TMIMS-MS system²⁴, as well as with three models of vapor dopant induced mobility shifts: (I)
18 mobility shifts due to changes in gas composition in the absence of vapor dopant uptake, (II)
19 mobility shifts due to both gas composition changes and site-specific dopant uptake by the
20 analyte molecule (approximated via a Langmuir adsorption model), and (III) mobility shifts due
21 to both gas composition changes and site-unspecific dopant uptake by the analyte molecule
22 (approximated via a classical nucleation model). We find that peptide ions appear to uptake
23 isopropanol quite readily, with results in best agreement with model II, the site-specific binding
24 model. Conversely, tetraalkylammonium ions do not uptake isopropanol efficiently in the gas
25 phase, with results in best agreement model III, which assumes non-specific dopant uptake. In
26 the subsequent sections, details of the experiments performed are provided and results are
27 presented, followed by a derivation of the expected mobility shifts from each of the developed
28 models. Finally, model predictions are compared to measurements, with the intended goal of
29
30
31
32
33
34
35
36
37
38
39
40
41
42
43
44
45
46
47
48
49
50
51
52
53
54
55
56
57
58
59
60

1
2
3 demonstrating that the present model framework can be used to link observed mobility shifts to
4
5 the mechanism by which mobility shifts arise.
6
7
8
9

10 **2. EXPERIMENTAL METHODS**

11 *2.1. Materials*

12
13
14
15 The standard peptide mixture used in experiments was obtained from Sigma Aldrich, and
16
17 consisted of Glycyl-L-tyrosine (MW = 238.2 Da), Val-Tyr-Val (MW = 380 Da), Leu-Enkephalin
18
19 (MW = 556 Da), Met-Enkephalin (MW = 574 Da) and Angiotensin II (MW = 1046 Da, doubly
20
21 charged in the gas phase). A solution 50 $\mu\text{g/ml}$ in concentration was prepared in 50% deionized
22
23 water, 48% methanol and 2% acetic acid. Tetraheptylammonium bromide (THABr) was added
24
25 to the solution at a nominal concentration of 0.5 mM, to be used as an internal mobility
26
27 standard²⁷. HPLC-grade isopropanol was used as the dopant in measurements.
28
29
30
31
32
33

34 *2.2 Experimental Setup*

35
36
37 A schematic of the ESI-TMIMS-MS system used in all measurements is shown in figure
38
39 1. The sample ions, produced via positive nano-ESI, were introduced directly into the TMIMS
40
41 cell electrostatically against counterflow; the nano-ESI source was floated above the TMIMS
42
43 inlet by 5 kV, which was necessary to maintain a stable Taylor cone²⁸. Coupled with the
44
45 counterflow, an atmospheric pressure desolvation flow was employed to promote ESI droplet
46
47 evaporation, and further promoted ion transmission from nano-ESI source into the TMIMS
48
49 analyzer. A focusing ring electrode with an applied potential 2kV above the TM-IMS inlet was
50
51 also used to guide the ion beam to the center of the TM-IMS inlet, which improved instrument
52
53 resolution. The design and operation of the TMIMS system is described in detail previously.²⁴
54
55
56
57
58
59
60

1
2
3 Briefly, the system employed in this work consisted of two TMIMS cells, and can facilitate both
4 one-dimensional and two-dimensional mobility separations. Full operation of these two
5 chambers requires the use of three axial electrodes and four deflector electrodes. The inlet axial
6 electrode (figure 1) and intermediate electrode are powered by an Applied Kilovolts high voltage
7 amplifier, while the outlet axial electrode is grounded. The deflector electrodes are powered by
8 two Matsuda high voltage and high speed amplifiers. Here, the first TMIMS cell was operated in
9 a transmission only (transparent) mode, with the second cell used for mobility separation. With
10 this mode of operation, the inlet axial voltage was ~16kV, the intermediate was ~8kV and the
11 outlet was grounded. The DC component of the deflector voltages were ~12kV for first cell and
12 ~4kV for second cell. No AC component was applied to the first cell (hence its deflector
13 electrodes were held fixed close to the same voltage, with a slight DC component employed to
14 optimize transmission), while the AC component of the second cell was 10 kV peak to peak, and
15 the frequency was varied from 200 to 1000 Hz to facilitate mobility separation. Gas flows were
16 also introduced in both cells, 3 l min⁻¹ in the first cell and 1.5 l min⁻¹ in second cell. 3.2 l min⁻¹
17 of flow exits the first cell inlet (as the counterflow), 0.8 l min⁻¹ exits as exhaust flow (0.5 l min⁻¹
18 in the second cell), and 0.5 l min⁻¹ passes to the mass spectrometer inlet. The mass spectrometer
19 was a Thermo Scientific LTQ XL linear ion trap mass spectrometer.
20
21
22
23
24
25
26
27
28
29
30
31
32
33
34
35
36
37
38
39
40
41
42

43 Isopropanol vapor was introduced as the dopant into the second stage via the inlet flow,
44 with the isopropanol vapor concentration controlled via syringe pump-membrane system as
45 described elsewhere.²⁴ The temperature of the second TMIMS cell was close to 300 K for all
46 measurements and the pressure was near atmospheric pressure. Under these conditions, the
47 isopropanol gas phase concentration was varied from 0 to 2% (by partial pressure/ partial
48 volume), which corresponds isopropanol saturation ratios of $S = 0 - 0.4$. TMIMS-MS spectra, in
49
50
51
52
53
54
55
56
57
58
59
60

1
2
3 which the AC frequency in the second TMIMS cell was scanned and the detected signal of a
4 specific ion was monitored in the mass spectrometer, were collected for 5 separate isopropanol
5 concentrations. For each ion, measurements were repeated (once stable operating conditions at a
6 given isopropanol vapor concentration) 10 times or more; a negligible difference (less than 2%)
7 in mobility was observed between measurements.
8
9
10
11
12
13
14
15
16
17

18 3. RESULTS & DISCUSSION

19 3.1. Measured Mobilities

20
21 In TMIMS measurements, mobility is linked to the frequency of the AC-component of
22 the deflector electrodes, with the mobility of the ions transmitted linearly proportional to
23 frequency. This is distinct from both drift tube mobility spectrometers²⁹ and differential
24 mobility analyzers³⁰, as in these instruments, the swept parameter (drift time and voltage,
25 respectively) is linearly proportional to inverse mobility. In addition, in TMIMS, ions not only
26 of a single mobility, but also with mobilities of K_0/n (where n is a positive integer and K_0 is
27 baseline mobility) are transmitted through instrument at a given frequency. Therefore, multiple
28 peaks are anticipated for a particular structural isomer, and spectra need to be interpreted
29 accounting for ion transmission at multiple frequencies. Figure 2 displays TMIMS spectra
30 (signal as a function of frequency) for the 5 examined ions at all 5 employed isopropanol
31 concentrations (denoted by the isopropanol saturation ratio). For each ion, multiple peaks are
32 present in spectra. Nonetheless, we can identify only one structural isomer per ion as each peak
33 present is found at a location proportional to a particular baseline frequency (ν_0 , which upon
34 calibration reveals K_0). Evident in spectra is that the resonant peaks for each ion do not have
35 equal signal intensities; this arises because of the frequency dependent transmission of TMIMS
36
37
38
39
40
41
42
43
44
45
46
47
48
49
50
51
52
53
54
55
56
57
58
59
60

1
2
3 systems.²⁶ For systematic calibration, we elected to infer mobilities (based upon the TMIMS
4 spectrum for the tetraheptylammonium ion in the absence of isopropanol) using the lowest
5 frequency peak in each spectrum, and vertical lines are present in figure 2 to identify each of the
6 lowest frequency peaks. The addition of isopropanol led to a shift in all ions peak to lower
7 frequencies and hence lower mobilities. This is indicative of either isopropanol uptake by ions,
8 which would increase their cross sections and therefore decrease their mobilities, or indicative
9 that isopropanol-ion collisions lead to an appreciable shift in collision cross sections. Also in
10 figure 2, larger shifts in TMIMS spectra peak locations are apparent at lower isopropanol
11 saturation ratios. In figure 3a, we plot the inferred ion mobility as a function of saturation ratio.
12 For all peptides, we observe sharp decreases in the mobility upon introduction of isopropanol,
13 but above a critical saturation (near $S = 0.04$ in all circumstances) little shift in mobility is
14 observed with increasing saturation ratio. The observed decreases in mobility can be contrasted
15 with the observations made by Vidal-de-Miguel et al²⁴ for tetraalkylammonium ions. For
16 comparison we plot their results in figure 3b, and in this figure a near-linear decrease in mobility
17 is observed with increasing saturation ratio, and relative shifts in mobility are noticeably lower
18 than is observed for peptide ions. Clearly, isopropanol differentially influences these two ions
19 types; this behavior can be rationalized through the development of mobility shifts models,
20 which are presented in the next section.
21
22
23
24
25
26
27
28
29
30
31
32
33
34
35
36
37
38
39
40
41
42
43
44
45
46
47

48 *3.2. Models of Vapor Dopant Induced Mobility Shifts*

49

50
51 Upon collision with an ion, isopropanol (or any vapor dopant) may either be reemitted
52 from the ion surface (much like a bath gas molecule) or may bind to the surface, to be reemitted
53 at a later time. The influence of both vapor dopant impingement and reemission as well as
54
55
56
57
58
59
60

binding must be considered in predicting shifts in mobilities. For simplicity, we first develop a model of mobility shift neglecting vapor dopant binding to ions (model I); in this instance vapor dopants would shift mobilities if they were present in high enough concentrations for momentum transfer³¹⁻³⁴ from vapor dopant molecules to ions to be significant. The mobility of an ion, K , can be expressed by the equation:

$$K = \frac{ze}{f} \quad (1)$$

where f is the friction factor, z is the ion charge state, and e is the unit electron charge. In the free molecular regime (applicable when the mean free path of the bath gas is much larger than the ion³⁵, which is the case for peptide and tetraalkylammonium ions), in a pure gas (gas composition "0"), the friction factor is given by the equation:

$$f = \frac{4}{3} \rho_{b,0} \bar{c}_0 \Omega_{0,0} \quad (2)$$

where $\rho_{b,0}$ is the bath gas mass density in the absence of vapor dopant, \bar{c}_0 is the mean thermal speed of the ion-gas molecule reduced mass³⁶, and $\Omega_{0,0}$ is the collision cross section of the ion in question, in the absence vapor dopants, and without any bound vapor dopants. With a second gas added (the vapor dopant), the friction in the free molecular regime (wherein gas molecule do not interact with one another in close proximity to the ion) can be calculated as:

$$f = \frac{4}{3} \rho_{b,S} \bar{c}_0 \Omega_{0,0} + \frac{4}{3} \rho_S \bar{c}_v \Omega_{0,v} \quad (3)$$

where $\rho_{b,S}$ is the bath gas density at vapor dopant saturation ratio S , ρ_S is the vapor dopant mass density, \bar{c}_v is the mean thermal speed of the ion-vapor dopant reduced mass, and $\Omega_{0,v}$ is the collision cross section of the bare ion if it was immersed in purely the vapor dopant as a bath gas. Combining equations (1) and (3), for model I, the ratio of the mobility in the absence of vapor dopant (K_i) to the mobility at saturation ratio S (K_S) is given as:

$$\frac{K_i}{K_S} = \left(\frac{\rho_{b,s}}{\rho_{b,0}} + \frac{\rho_S}{\rho_{b,0}} \left(\frac{\mu_{0,0}}{\mu_{0,v}} \right)^{1/2} \frac{\Omega_{0,v}}{\Omega_{0,0}} \right) \quad \text{model I} \quad (4)$$

where $\mu_{0,0}$ is the reduced mass of the ion-bath gas system, and $\mu_{0,v}$ is the reduced mass of the ion-vapor dopant system. Because the term $\frac{\rho_{b,s}}{\rho_{b,0}}$ remains close to unity for low to modest saturation ratios (for most vapor dopants), equation (4) predicts a near linear increase in the ratio K_i/K_S with increasing vapor dopant density, with the slope proportional to $\frac{\Omega_{0,v}}{\Omega_{0,0}}$. Predictions of mobility shifts therefore require the development of models of ion collision cross sections not only in bath gas, but in vapor dopants, which are typically much more massive than gas molecules, and further may have appreciable dipole moments. Ideally, such influences would be incorporated into direct gas molecule to ion momentum transfer calculations, as are described by Shvartsburg & coworkers^{34, 37-40} or Larriba & coworkers^{32, 33, 41}. Discussed following the presentation of models II & III, here we invoke approximate physical size based models of collision cross sections for ions.

Converse to model I, in models II & III we consider that upon collision a vapor dopant may bind with the ion and further may dissociate (evaporate) from the surface at a later time. We assume that while mobility measurement is carried out, there are a sufficient number of ion-vapor dopant molecule collisions for the ion to equilibrate with the background vapor, such that each ion probes the equilibrium distribution of bound vapor dopant molecules. Following the arguments of Oberreit et al⁴² while simultaneously accounting for vapor dopant to ion momentum transfer, ion mobility at a particular saturation ratio can be predicted with the equation:

$$K_S = \frac{3ze}{4} \sum_{g=0}^{\infty} \frac{P_g}{\rho_{b,s} \bar{c}_{0,g} \Omega_{g,0} + \rho_S \bar{c}_{v,g} \Omega_{g,v}} \quad (5)$$

where P_g is the probability (at equilibrium, and model dependent) that the ion has g vapor dopant molecules bound to its surface at any instant in time, $\bar{c}_{0,g}$ is the mean thermal speed of the reduced mass of a bath gas molecule and the ion with g vapor molecules bound, $\bar{c}_{v,g}$ is the mean thermal speed of the reduced mass of a vapor dopant molecule and the ion with g vapor molecules bound, $\Omega_{g,0}$ is the collision cross section of the ion with g vapor molecules bound in the bath gas, and $\Omega_{g,v}$ is the collision cross section of the ion with g vapor molecules bound if it were immersed in the vapor dopant. Equation (5) is additionally applicable to model I; in model I simply $P_0 = 1$ and $P_g = 0$ for $g > 0$ is assumed. The ratio K_i/K_S can be calculated using the equation:

$$\frac{K_i}{K_S} = \frac{1}{\sum_{g=0}^{\infty} \left(\frac{P_g}{\frac{\rho_{b,S} \bar{c}_{0,g} \Omega_{g,0}}{\rho_{b,0} \bar{c}_0 \Omega_{0,0}} + \frac{\rho_{v,S} \bar{c}_{v,g} \Omega_{g,v}}{\rho_{v,0} \bar{c}_0 \Omega_{0,0}}} \right)} \quad \text{models II \& III} \quad (6)$$

To apply equation (6), in addition to predicting collision cross sections for ions with varying numbers of vapor dopant molecules bound in both the bath gas and the vapor dopant (i.e. predictions of $\Omega_{g,0}$ and $\Omega_{g,v}$), models for P_g are required. In model II, we invoke the Langmuir adsorption model, which considers that vapor dopants can bind at specific sites on the ion surface, with a total of g_{max} available sites (an integer value). As shown in the supplemental information, this model leads P_g described by the equations:

$$P_0 = \frac{1}{1 + \sum_{j=1}^{g_{max}} (\gamma S)^j \prod_{k=1}^j \left(\left(\frac{1 - \frac{k-1}{g_{max}}}{\frac{k}{g_{max}}} \right) \left(\frac{\mu_{k,v}}{\mu_{k-1,v}} \right)^{1/2} \left(\frac{r_{k-1} + r_v}{r_k + r_v} \right)^2 \eta[\psi_{D,k-1}] \right)} \quad (7a)$$

$$P_g = \frac{(\gamma S)^g \prod_{j=1}^g \left(\left(\frac{1 - \frac{j-1}{g_{max}}}{\frac{j}{g_{max}}} \right) \left(\frac{\mu_{j,v}}{\mu_{j-1,v}} \right)^{1/2} \left(\frac{r_{j-1} + r_v}{r_j + r_v} \right)^2 \eta[\psi_{D,j-1}] \right)}{1 + \sum_{j=1}^{g_{max}} (\gamma S)^j \prod_{k=1}^j \left(\left(\frac{1 - \frac{k-1}{g_{max}}}{\frac{k}{g_{max}}} \right) \left(\frac{\mu_{k,v}}{\mu_{k-1,v}} \right)^{1/2} \left(\frac{r_{k-1} + r_v}{r_k + r_v} \right)^2 \eta[\psi_{D,k-1}] \right)} \quad g \geq 1 \quad (7b)$$

where $\mu_{k,v}$ is the reduced mass of the vapor dopant and ion with k vapor molecules (note k and j are simply as indices in summations) bound, r_k is the effective radius of the ion with k vapor molecules bound, $\eta[\psi_{D,k}]$ is dimensionless enhancement factor for the collision cross section of an ion with k vapor molecules bound and a vapor molecule, brought about by the ion induced dipole potential⁴³, and finally γ is the ratio of the saturation vapor pressure of the dopant to the vapor pressure above a binding site on the ion. While inference of r_k and $\eta[\psi_{D,k}]$ are described in the subsequent section, γ , along with g_{max} , is a fit parameter in equations (7a) & (7b); hence model II has two fit parameters built within it.

The Langmuir model runs converse to the model traditionally invoked when predictions of homogenous nucleation⁴⁴ or ion induced nucleation⁴⁵ of condensed phase species from vapor phase precursor are made. In these instances, a combination of surface energy effects (capillarity effects, as described by the Kelvin equation⁴⁶) and the influence of ion charge state (the Thomson effect) are commonly considered in determining the rate of vapor dissociation from an ion surface⁴⁷. In model III, we also consider the combined Kelvin and Thomson influences (which typically termed the classical nucleation model). As shown in the supplemental information, this leads to P_g described by the equations:

$$P_0 = \frac{1}{1 + \sum_{j=1}^{g_{max}} S^j \prod_{k=1}^j \left(\exp\left(\frac{\Delta E_k}{k_B T}\right) \left(\frac{\mu_{k,v}}{\mu_{k-1,v}}\right)^{1/2} \left(\frac{r_{k-1} + r_v}{r_k + r_v}\right)^2 \eta[\psi_{D,k-1}] \right)} \quad (8a)$$

$$P_g = \frac{S^g \prod_{j=1}^g \left(\exp\left(\frac{\Delta E_j}{k_B T}\right) \left(\frac{\mu_{v,j}}{\mu_{v,j-1}}\right)^{1/2} \left(\frac{r_{j-1} + r_v}{r_j + r_v}\right)^2 \eta[\psi_{D,j-1}] \right)}{1 + \sum_{j=1}^{g_{max}} S^j \prod_{k=1}^j \left(\exp\left(\frac{\Delta E_k}{k_B T}\right) \left(\frac{\mu_{k,v}}{\mu_{k-1,v}}\right)^{1/2} \left(\frac{r_{k-1} + r_v}{r_k + r_v}\right)^2 \eta[\psi_{D,k-1}] \right)} \quad g \geq 1 \quad (8b)$$

where $k_B T$ is the thermal energy, and ΔE_k is the change in enthalpy of an ion upon the sorption of an additional vapor dopant molecule (from $k-1$ to k molecules bound), calculated as:

$$\Delta E_k = -\sigma \delta A_k - \frac{(ze)^2}{8\pi\epsilon_0} \left(1 - \frac{1}{\epsilon_r}\right) \delta \left(\frac{1}{r_k}\right) \quad (9)$$

In equation (9), σ is the surface tension of the vapor dopant (as a liquid), ϵ_0 is the permittivity of free space, ϵ_r is the vapor dopant dielectric constant, δA_k is the change in surface area upon sorption from $k-1$ to k vapor molecules and $\delta \left(\frac{1}{r_k}\right)$ is the change in the inverse radius of an ion upon sorption from $k-1$ to k vapor molecules. The first term in equation (9) represents the Kelvin influence, while the second represents the Thomson (charge) influence. Unlike model II, there are no free parameters in model III, unless mobility shift data themselves are used to infer bulk properties, such as the surface tension of the vapor dopant (i.e. these parameters could be fit to measurements). Via comparison of equations (7a) & (7b) to equations (8a) & (8b), it becomes clear that in the Langmuir adsorption model (model II) the uptake of vapor is entropically driven (there is no enthalpy term, i.e. no exponential term), while in model III the enthalpy terms (the Kelvin and Thomson influences, respectively) have the largest influence on P_g . In addition to the models developed here, hybrid models, incorporating aspects of the both Langmuir-type adsorption as well as classical nucleation elements can be developed, and further more detailed information on binding can be incorporated for alternative mobility shift predictions.

To compare models II & III, figures 4a and 4b display plots of P_g values for Angiotensin II predicted by model II (with the maximum available number of binding sites, $g_{max} = 13$, and the ratio of the saturation vapor pressure of the dopant to the vapor pressure above a binding site on the ion, $\gamma = 23$; these values, as shown subsequently, are chosen to qualitatively fit measurements) and model III respectively. Comparison of these two figures shows that for small saturation ratios, model II predicts a larger degree of vapor dopant binding. However, because model III predictions are not bounded by g_{max} , at higher saturation ratios, this model predicts a greater extent of vapor dopant binding. In figure 5, for Angiotensin II, predictions of K_i/K_S as a

1
2
3 function of S are provided using models I, II, and III over a wide saturation ratio change,
4
5 revealing that model I predicts a near linear increase in K_i/K_S , model II predicts a concave
6
7 downward function where a maximum K_i/K_S value is reached at high S (dependent upon g_{\max}),
8
9 and model III (when incorporating both the Kelvin and Thomson effects) predicts smaller shifts
10
11 than model III at low saturation ratios, but larger shifts as the saturation ratio increases. Uptake
12
13 in model III is largely facilitated via the Thomson effect (the term related to ion charge); in
14
15 figure 5 we also plot model III predictions excluding the Thomson effect and find that below a
16
17 critical saturation ratio, little-to-no vapor uptake is observed, with predictions in line with model
18
19 I (and homogenous nucleation above this critical saturation ratio).
20
21
22
23
24
25
26

27 *3.3. Ion Collision Cross Section and Physical Size Models*

28
29 A number of physical parameters for ions and vapor molecules must be known to utilize
30
31 models I, II, & III. First, for the collision cross sections, we remark again that extremely
32
33 accurate collision cross section predictions, particularly for collision cross sections in vapor
34
35 dopants, would require the use of gas molecule scattering calculation procedures with detailed
36
37 consideration of ion structure, gas molecule/vapor dopant structure, and the potential interactions
38
39 between ions and impinging molecules³². However, a number of studies^{5, 12, 48} show that even
40
41 for small molecules, it is possible to approximate the collision cross sections of ions by modeling
42
43 all ions and vapor molecules as spheres with bulk density. We elect to use this approach here to
44
45 directly compare to experiments. While we do not advocate the use of such approximations in
46
47 all circumstances (e.g. in instances where extremely accurate values of the collision cross section
48
49 are of interest), because all collision cross sections are normalized in calculations (by the bare
50
51
52
53
54
55
56
57
58
59
60

ion collision cross section in pure bath gas) we do not believe the spherical approximation invalidates our comparison to experiments.

To infer the collision cross section of an ion with k dopant molecules bound, in pure bath gas ($\Omega_{k,0}$), we invoke a modified form of the Stokes-Millikan equation's^{33, 49} free molecular limit, linking the collision cross section to the ion radius (r_k):

$$\Omega_{k,0} = \xi\pi(r_k + r_b)^2 L(\psi_{pol,k}) \quad (10)$$

where $\xi = 1.36$ is the momentum scattering factor deriving from the measurements of Millikan⁵⁰, r_b is the bath gas effective radius (assumed based on prior work to be 0.155 nm at the measurement temperature¹²), and $L(\psi_{pol,k})$ is a collision cross section enhancement factor accounting for the ion-induced dipole potential between bath gas molecules (diatomic nitrogen, with polarizability $\alpha_{pol} = 1.71 \times 10^{-30} \text{ m}^3$) and the ion, given by Larriba & Hogan³³:

$$L(\psi_{pol,k}) = 1 + \psi_{pol,k} \left(\frac{1}{3.1} + \frac{1}{\xi} \left(\frac{1}{16} + \frac{4}{33} \psi_{pol,k} \right) \right) \text{ if } \psi_{pol,k} \leq 1 \quad (11a)$$

$$L(\psi_{pol,k}) = 1 + \psi_{pol,k} \left(\frac{1}{4} - \frac{2.3}{1000} \psi_{pol,k} + \frac{1}{\xi} \left(\frac{9}{56} - \frac{6.8}{1000} \psi_{pol,k} \right) \right) \text{ if } \psi_{pol,k} > 1 \quad (11b)$$

wherein $\psi_{pol,k}$ is the polarization to thermal energy ratio:

$$\psi_{pol,k} = \frac{\alpha_{pol} z^2 e^2}{8\pi\epsilon_0 k_B T (r_k + r_b)^4} \quad (11c)$$

For the ion collision cross section immersed in the vapor dopant we analogously use the relationship

$$\Omega_{k,v} = \xi\pi(r_k + r_v)^2 \eta(\psi_{D,k}) \quad (12a)$$

where $\eta(\psi_D)$ is an enhancement factor in collision cross section considering the ion-dipole potential (significant because vapor dopants have non-negligible dipole moments, μ_D), and $\psi_{D,k}$ is the ion-dipole energy to thermal energy ratio:

$$\psi_{D,k} = \frac{ze\mu_D}{4\pi\epsilon_0 k_B T (r_k + r_v)^2} \quad (12b)$$

Here, we use the same collision cross section enhancement function $\eta(\psi_{D,k})$ in equations (7a), (7b), (8a), (8b), & (12a); in equations (7-8) this function arises because of the ion-dipole enhancement in ion vapor dopant collision rate for the incorporation of new dopant molecules to the cluster (mass transfer collision cross section), while in equation (12a), it is used to account for enhanced momentum transfer. Strictly, two separate functions should be applied in these instances. However, we are not aware of any prior analysis of the ion-dipole potential influence on momentum transfer, hence our choice to use the same function $\eta(\psi_{D,k})$ to account for ion-dipole influences in both mass transfer (collision rate) and momentum transfer. Following Su & Bowers⁴³, we calculate $\eta(\psi_{D,k})$ with the equation:

$$\eta(\psi_{D,k}) = 1 + C\psi_{D,k} \quad (12c)$$

with $C = 0.6$ (note $C = 1$ corresponds to complete dipole alignment, and $C = 0$ corresponds to no dipole alignment). Combining equations (10-12) leads to:

$$\frac{\Omega_{k,0}}{\Omega_{0,0}} = \frac{(r_k + r_v)^2 L(\psi_{pol,k})}{(r_0 + r_b)^2 L(\psi_{pol,0})} \quad (13a)$$

$$\frac{\Omega_{k,v}}{\Omega_{0,0}} = \frac{(r_k + r_v)^2 \eta(\psi_{D,k})}{(r_0 + r_b)^2 L(\psi_{pol,0})} \quad (13b)$$

Finally, to calculate r_k , r_b , and r_v , we treat all ions and gas molecules as spheres, with the properties utilized (based on assumed bulk densities) provided in tables 1 & 2, respectively.

Values of r_k are calculated using the equation:

$$r_k = (r_0^3 + kr_v^3)^{1/3} \quad (13c)$$

3.4. Model Comparison to Experiments

Despite the use of numerous approximations in calculations, we find that developed models can be fit well to experimental results in many circumstances. Specifically in figure 6, we plot the ratio K_i/K_S as a function of S for peptide ions and compare to model II predictions with fit values of g_{max} and γ (noted on the figure). With the exception of Val-Tyr-Val (380 Da), we find that g_{max} and γ both increase with increasing peptide mass, in-line with *a priori* expectations (larger ions should have more available “sites” for vapor binding, and further should have reduced vapor pressures above their surfaces). Because of the good agreement found, we suggest that for each of the examined ions, model II predictions (with fit parameters) can henceforth be used to predict the extent of uptake for ions with reasonable accuracy (near 300 K). Significantly weaker agreement is found with model III predictions for peptide ions, as depicted in the supplemental information. This suggests that bulk approximations for isopropanol and peptides are inappropriate in describing ion-vapor molecule interactions.

Unlike peptide ion mobility shifts, tetraalkylammonium ion mobility shifts are not found to agree well with model II. This is immediately evident because model II does not predict a linear relationship between mobility shift and saturation ratio, as is observed for these ions. However, the near linear shift in mobility is in-line with model III predictions. In figure 7, the ratio K_i/K_S is plotted as a function of S for tetraalkylammonium ions (from Vidal-de-Miguel et al²⁴) and compared to model I & III (both with and without consideration of the Thomson effect). For all ions, we find the best agreement with model III predictions including the Thomson effect. Considering the approximations made in collision cross section modeling and the lack of fit parameters in model III, the agreement observed suggests that isopropanol binds non-specifically

1
2
3 to tetraalkylammonium ions, with binding coefficients close to the expected values from
4
5 classical theory.
6
7
8
9

10 4. CONCLUSIONS

11
12 We examine shifts in the mobilities of peptide ions upon introduction of isopropanol into
13 a TMIMS cell. Contrary to what was found in a recent study²⁴ of tetraalkylammonium ions, we
14 find that peptide ions rapidly shift to lower values at low saturation ratios, but shifts cease with
15 increasing saturation ratio. To explain the differing levels of shift observed for different ion
16 types, we have developed models predicting ion mobility shifts due to both vapor dopant uptake
17 by ions, as well as direct vapor dopant-ion momentum transfer. Based on the comparison of
18 model predictions to measurements, we conclude that isopropanol appears to bind peptide ions in
19 a manner explained by the Langmuir adsorption model, while isopropanol interactions with
20 tetraalkylammonium ions are better explained by classical nucleation theory (non-specific
21 binding). While we find the presented models are an appropriate framework by which to model
22 vapor dopant induced mobility shifts, we also note that future model development will be
23 necessary to better predict mobility shifts. The three applied models are derived with very
24 specific assumptions regarding the nature of vapor dopant-ion interaction; model I assumes
25 vapor molecules never bind to ion surfaces, model II assumes that molecules bind only at a finite
26 number of specific sites all of which are identical to one another, and finally model III assumes
27 that bulk properties apply to vapor molecules and ions, and that vapor uptake on the molecular
28 scale can be described in a manner expected for a spherical, homogeneous droplet. None of
29 these models would rigorously apply to any vapor-ion system, and they instead represent limiting
30 cases which can be expanded upon in the development of more details models. For example,
31
32
33
34
35
36
37
38
39
40
41
42
43
44
45
46
47
48
49
50
51
52
53
54
55
56
57
58
59
60

1
2
3 model II, assuming Langmuir-like adsorption, could be modified to consider enthalpic
4 influences, and additionally binding site dependent energies (which may be measured or derived
5 quantum chemical computations). Models could also be developed in which site-specific
6 binding is considered for low number of sorbed vapor molecules, while site-unspecific binding is
7 considered for larger numbers of vapor molecules (which would approximate monolayer
8 formation, followed by subsequent uptake). Even with such complications introduced, it should
9 be noted that equation (6), as expressed here, would still accurately describe mobility shifts, it is
10 only the relationship for P_g which would be modified. Finally, we remark that in principle,
11 mobility shift measurements themselves may be able to yield information on P_g and hence the
12 equilibrium binding coefficients for vapor molecules.
13
14
15
16
17
18
19
20
21
22
23
24
25
26
27
28

29 5. ACKNOWLEDGEMENTS

30
31 V.R. acknowledges the Joachim and Yuko Heberlein scholarship, which provided
32 support for his visit to SEADM. Model development was additionally supported by US National
33 Science Foundation Grant CHE- 1011810. GVM acknowledges the Eurostars program (project
34 IMMA) for supporting the development of the TMIMS, and Thermo Fisher Scientific for the
35 loan of the LTQ-MS.
36
37
38
39
40
41
42
43
44
45

46 6. SUPPLEMENTAL INFORMATION

47
48 Derivations of the P_g functions employed in model II and model III, model III
49 comparisons to peptide measurements, and a variable dictionary are available online.
50
51
52
53
54
55
56
57
58
59
60

7. REFERENCES

1. S. I. Merenbloom, S. L. Koeniger, S. J. Valentine, M. D. Plasencia and D. E. Clemmer, *Analytical Chemistry*, 2006, 78, 2802.
2. L. Tao, J. R. McLean, J. A. McLean and D. H. Russell, *J Am Soc Mass Spectrom*, 2007, 18, 1232-1238.
3. Z. Berant and Z. Karpas, *Journal of the American Chemical Society*, 1989, 111, 3819-3824.
4. G. W. Griffin, I. Dzidic, D. I. Carroll, R. N. Stillwell, E. C. Horning, G. W. Griffin, I. Dzidic, D. I. Carroll, R. N. Stillwell and E. C. Horning, *Analytical Chemistry*, 1973, 45, 1204-1209.
5. C. Larriba, C. J. Hogan, M. Attoui, R. Borrajo, J. Fernandez-Garcia and J. Fernandez de la Mora, *Aerosol Science and Technology*, 2011, 45, 453-467.
6. J. A. McLean, *J Am Soc Mass Spectrom*, 2009, 20, 1775-1781.
7. P. Palma, G. Famigliini, H. Trufelli, E. Pierini, V. Termopoli and A. Cappiello, *Anal Bioanal Chem*, 2011, 399, 2683-2693.
8. J. L. Desantos-Garcia, S. I. Khalil, A. Hussein, Y. Hu and Y. Mechref, *Electrophoresis*, 2011, 32, 3516-3525.
9. P. V. Johnson, H. I. Kim, L. W. Beegle, I. Kanik, P. V. Johnson, H. I. Kim, L. W. Beegle and I. Kanik, *Journal of Physical Chemistry A*, 2004, 108, 5785.
10. M. F. Bush, Z. Hall, K. Giles, J. Hoyes, C. V. Robinson and B. T. Ruotolo, *Analytical Chemistry*, 2010, 82, 9557-9565.
11. C. J. Hogan and J. Fernandez de la Mora, *J Am Soc Mass Spectrom*, 2011, 22, 158-172.
12. B. K. Ku and J. Fernandez de la Mora, *Aerosol Science and Technology*, 2009, 43, 241-249.
13. A. Maiber, V. Premnath, A. Ghosh, T. A. Nguyen, M. Attoui and C. J. Hogan, *Physical Chemistry & Chemical Physics*, 2011, 13, 21630-21641.
14. A. Shvartsburg, K. Tang and R. Smith, *J Am Soc Mass Spectrom*, 2004, 15, 1487-1498.
15. A. A. Shvartsburg, *Differential ion mobility spectrometry : nonlinear ion transport and fundamentals of FAIMS*, Boca Raton : CRC Press, Boca Raton, 2009.
16. J. Puton, M. Nousiainen and M. Sillanpää, *Talanta*, 2008, 76, 978-987.
17. G. A. Eiceman, E. V. Krylov, N. S. Krylova, E. G. Nazarov and R. A. Miller, *Analytical chemistry*, 2004, 76, 4937.
18. H. Borsdorf, T. Mayer, M. Zarejousheghani and G. A. Eiceman, *Applied Spectroscopy Reviews*, 2011, 46, 472-521.
19. M. Zhu, B. Bendiak, B. Clowers and H. H. Hill, *Analytical and Bioanalytical Chemistry*, 2009, 394, 1853.
20. W. E. Steiner, S. J. Klopsch, W. A. English, B. H. Clowers and H. H. Hill, *Analytical chemistry*, 2005, 77, 4792.
21. M. Mäkinen, M. Nousiainen and M. Sillanpää, Hoboken, 2011, vol. 30, pp. 940-973.
22. G. A. Eiceman and J. A. Stone, *Analytical Chemistry*, 2004, 76, 390 A-397 A.
23. D. S. Levin, R. A. Miller, E. G. Nazarov and P. Vouros, *Analytical Chemistry*, 2006, 78, 5443-5452.
24. G. Vidal de Miguel, M. Macia, C. Barrios and J. Cuevas, *Anal. Chem.*, 2015, DOI: 10.1021/ac504178n, 150105110046005.
25. G. Vidal-de-Miguel, M. Macia and J. Cuevas, *Analytical chemistry*, 2012, 84, 7831-7837.

- 1
- 2
- 3
- 4 26. C. Barrios-Collado and G. Vidal-de-Miguel, *International Journal of Mass Spectrometry*, 2015, 376, 97-105.
- 5
- 6 27. S. Ude, J. Fernández de la Mora and B. A. Thomson, *Journal of the American Chemical Society*, 2004, 126, 12184-12190.
- 7
- 8 28. M. Yamashita and J. B. Fenn, *The Journal of Physical Chemistry*, 1984, 88, 4451-4459.
- 9 29. H. E. Revercomb and E. A. Mason, *Analytical Chemistry*, 1975, 47, 970-983.
- 10 30. E. O. Knutson and K. T. Whitby, *Journal of Aerosol Science*, 1975, 6, 443-451.
- 11 31. P. S. Epstein, *Physical Review*, 1924, 23, 710-733.
- 12 32. C. Larriba and C. J. Hogan, *Journal of Computational Physics*, 2013, 251, 344-363.
- 13 33. C. Larriba and C. J. Hogan, *The Journal of Physical Chemistry A*, 2013, 117, 3887-3901.
- 14 34. M. F. Mesleh, J. M. Hunter, A. A. Shvartsburg, G. C. Schatz and M. F. Jarrold, *J Phys Chem-Us*, 1996, 100, 16082-16086.
- 15 35. C. N. Davies, *Proceedings of the Physical Society*, 1945, 57, 259-270.
- 16 36. W. G. Vincenti and C. H. Kruger, *Introduction to Physical Gas Dynamics*, Krieger, Huntington, NY, 1975.
- 17 37. Y. Alexeev, D. G. Fedorov and A. A. Shvartsburg, *The Journal of Physical Chemistry A*, 2014, 118, 6763-6772.
- 18 38. A. A. Shvartsburg and M. F. Jarrold, *Chem Phys Lett*, 1996, 261, 86-91.
- 19 39. A. A. Shvartsburg, B. Liu, K. W. M. Siu and K. M. Ho, *Journal of Physical Chemistry A*, 2000, 104, 6152-6157.
- 20 40. A. A. Shvartsburg, S. V. Mashkevich, E. S. Baker and R. D. Smith, *Journal of Physical Chemistry A*, 2007, 111, 2002-2010.
- 21 41. C. Larriba-Andaluz and C. J. Hogan, *Journal of Chemical Physics*, 2014, 141, 194107.
- 22 42. D. R. Oberreit, P. H. McMurry and C. J. Hogan, *Phys Chem Chem Phys*, 2014, 16, 6968-6979.
- 23 43. T. Su and M. T. Bowers, *Journal of the American Chemical Society*, 1973, 95, 7609-7610.
- 24 44. J. L. Katz and M. D. Donohue, *A kinetic approach to homogeneous nucleation theory*, 1979.
- 25 45. S. P. Fisenko, D. B. Kane and M. S. El-Shall, *The Journal of chemical physics*, 2005, 123, 104704.
- 26 46. M. H. Factorovich, V. Molinero and D. A. Scherlis, *Journal of the American Chemical Society*, 2014, 136, 4508-4514.
- 27 47. S. K. Friedlander, *Smoke, Dust, and Haze*, Oxford University Press, New York, 2000.
- 28 48. H. Ouyang, C. Larriba-Andaluz, D. R. Oberreit and C. J. Hogan, *J Am Soc Mass Spectrom*, 2013, 24, 1833-1847.
- 29 49. J. Fernández-García and J. Fernández de la Mora, *J Am Soc Mass Spectrom*, 2013, 24, 1872-1889.
- 30 50. R. A. Millikan, *Physical Review*, 1923, 22, 1-23.
- 31
- 32
- 33
- 34
- 35
- 36
- 37
- 38
- 39
- 40
- 41
- 42
- 43
- 44
- 45
- 46
- 47
- 48
- 49
- 50
- 51
- 52
- 53
- 54
- 55
- 56
- 57
- 58
- 59
- 60

Table 1. A summary of the properties of ions used in model calculations.

Ion	Ion radius, r_0 (\AA^0)	Molecular weight (Da)	Charge state
Tetrapropylammonium	4.30	186	1
Tetrabutylammonium	4.70	242	1
Tetraheptylammonium	5.85	410	1
Tetradecylammonium	6.70	579	1
Tetradodecylammonium	7.00	691	1
Glycyl-L-Tyrosine	4.11	238	1
Val-Tyr-Val	4.99	380	1
Leu-Enkephalin	5.57	556	1
Met-Enkephalin	5.56	574	1
Angiotensin II	6.62	1046	2

Table 2. A summary of the properties of isopropanol used in model calculations.

Isopropanol properties	
Molecular weight (Da)	60
Effective radius (\AA^0)	3.12
Dipole Moment (D)	1.66
Vapor pressure at 300K (Pa)	5333
Surface Tension (N/m)	0.022

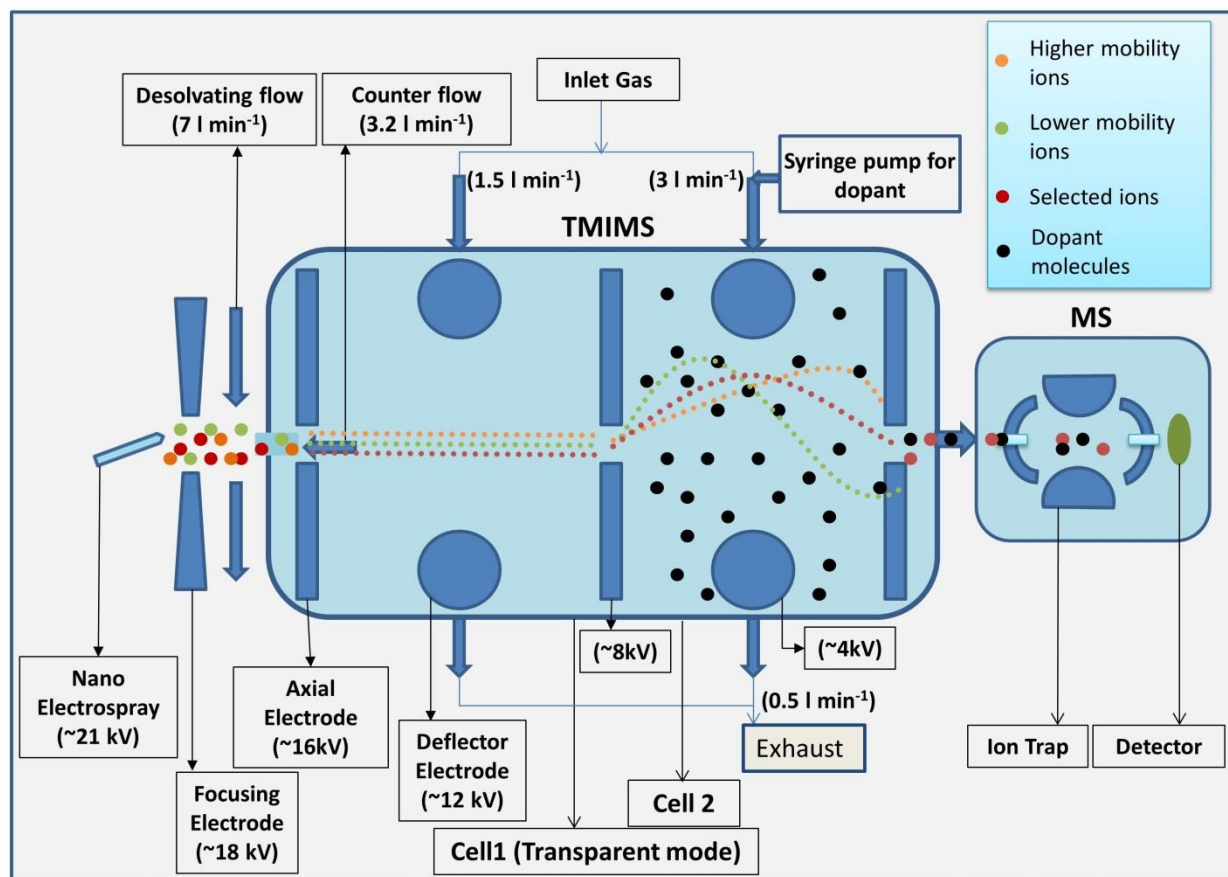


Figure 1. A schematic of the transversal modulation ion mobility spectrometry-mass spectrometry system employed in experiments.

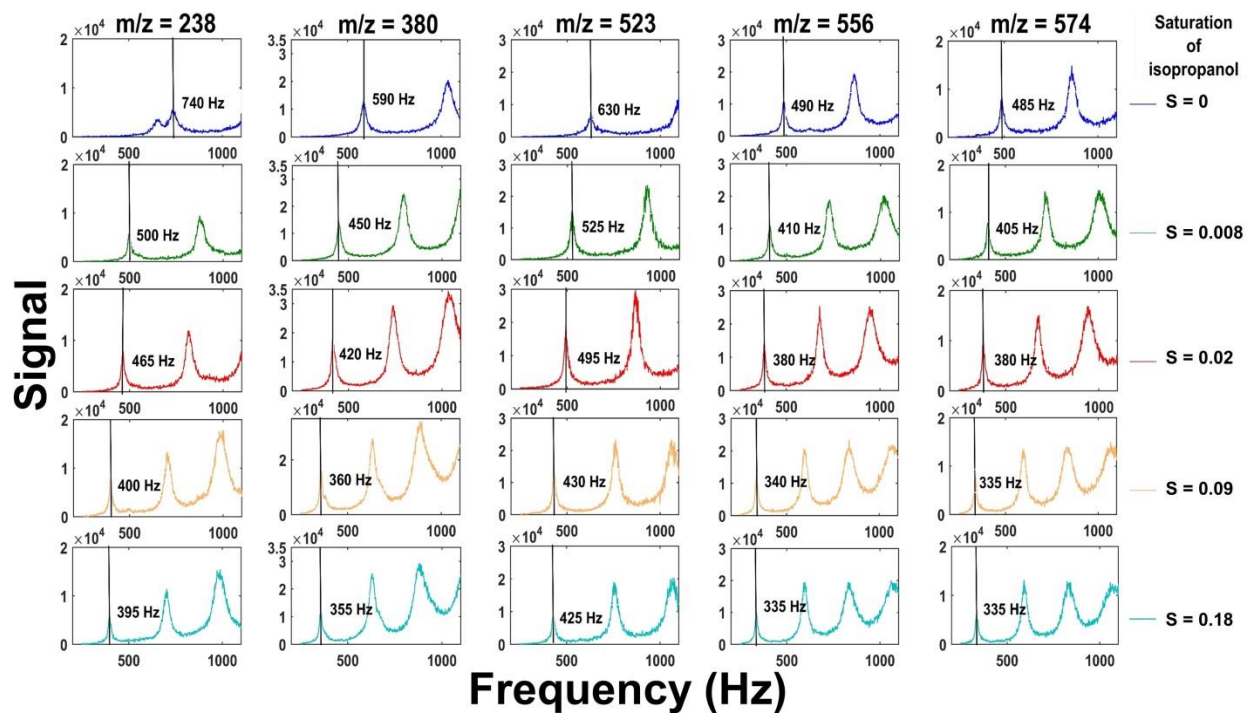


Figure 2. A summary of TMIMS spectra collected for 5 peptide ions at various isopropanol saturation ratios (at 300 K) in the TMIMS cell. The peaks used to infer ion mobilities are noted with vertical lines.

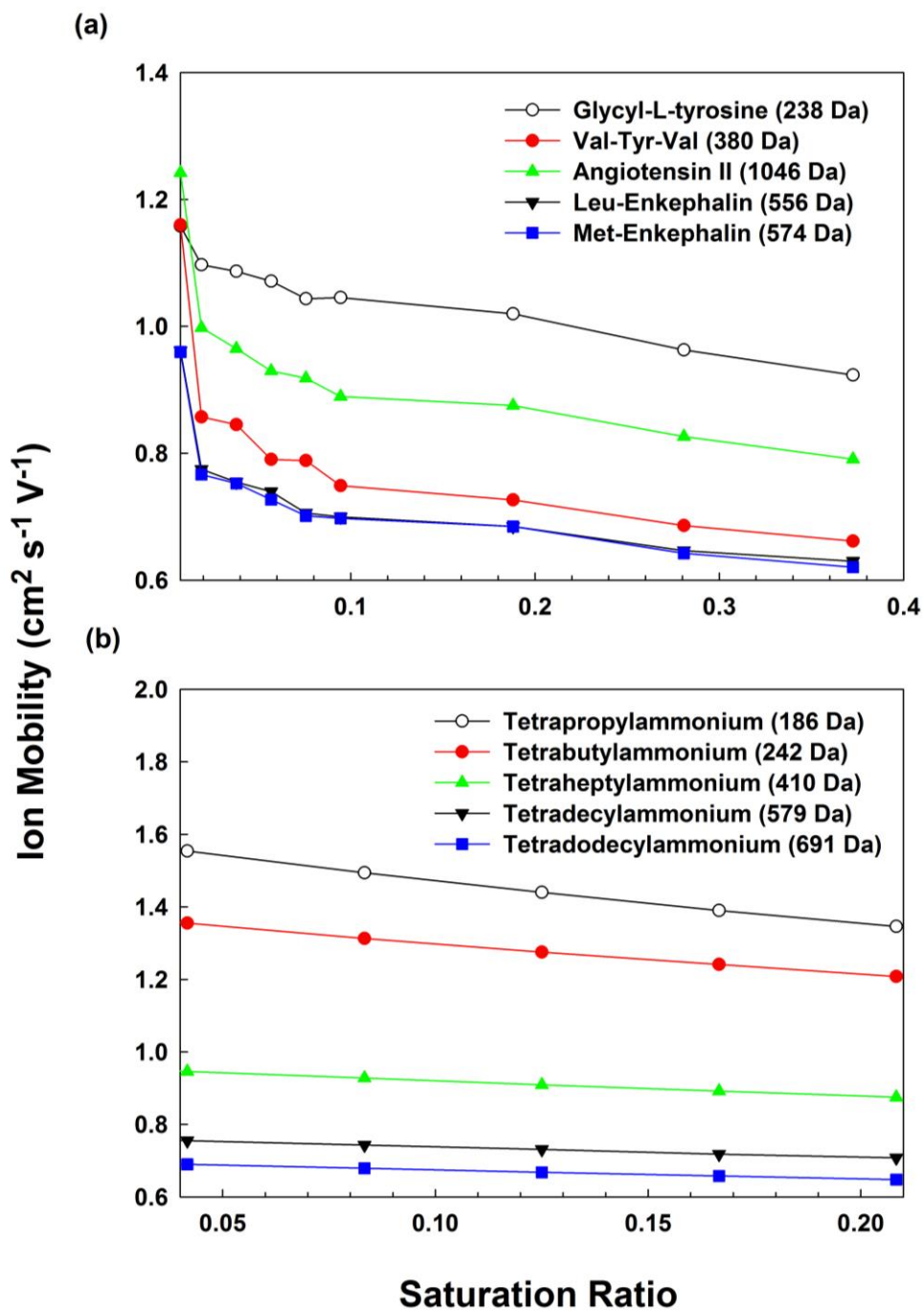


Figure 3. The mobilities of (a.) peptide ions and (b.) tetraalkylammonium ions (from Vidal-de-Miguel et al²⁴) as a function of isopropanol saturation ratio.

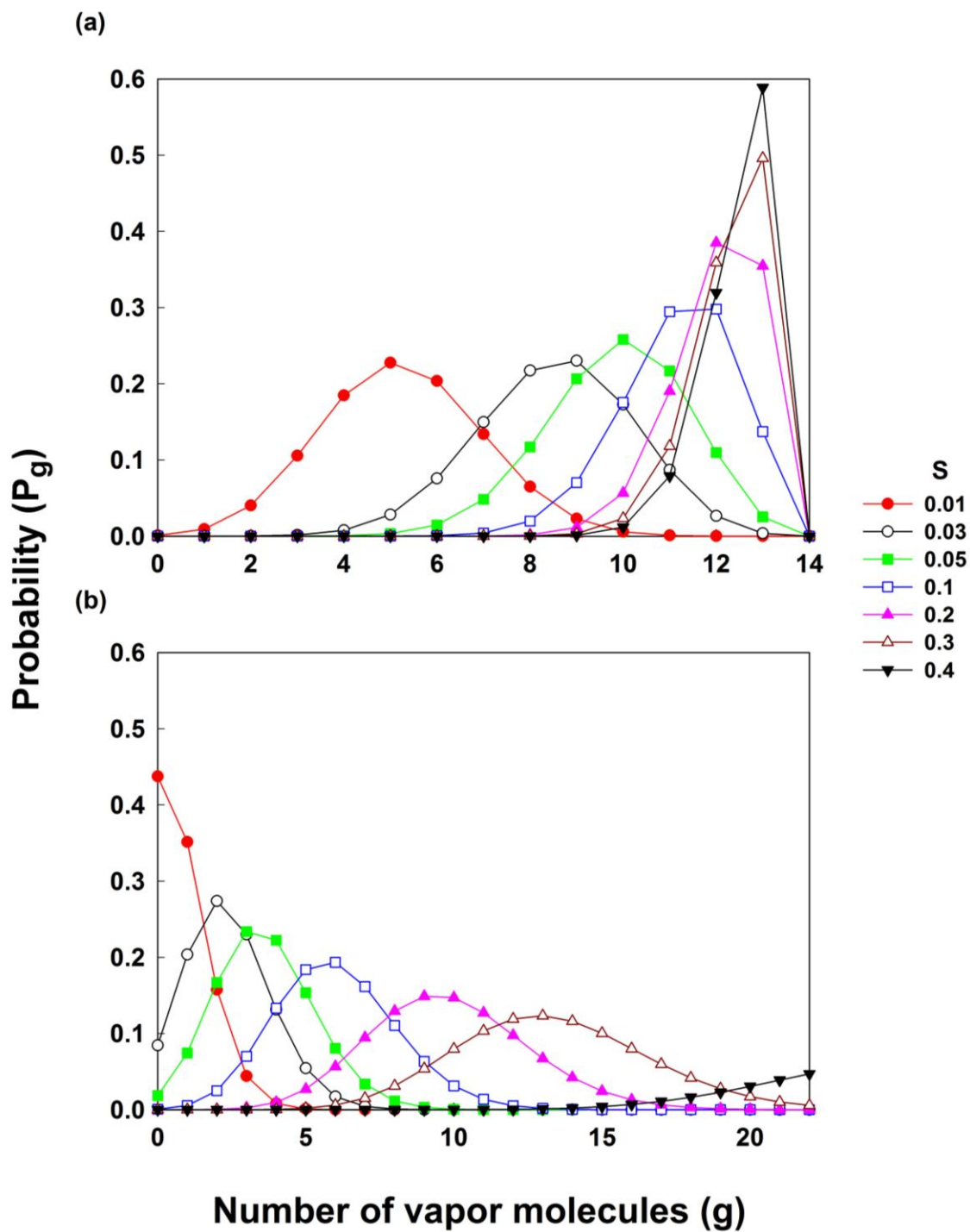


Figure 4. The probabilities P_g that an ion has g vapor molecules bound (at equilibrium) predicted by (a.) model II and (b.) model III as a function of g , for angiotensin II at various saturation ratios.

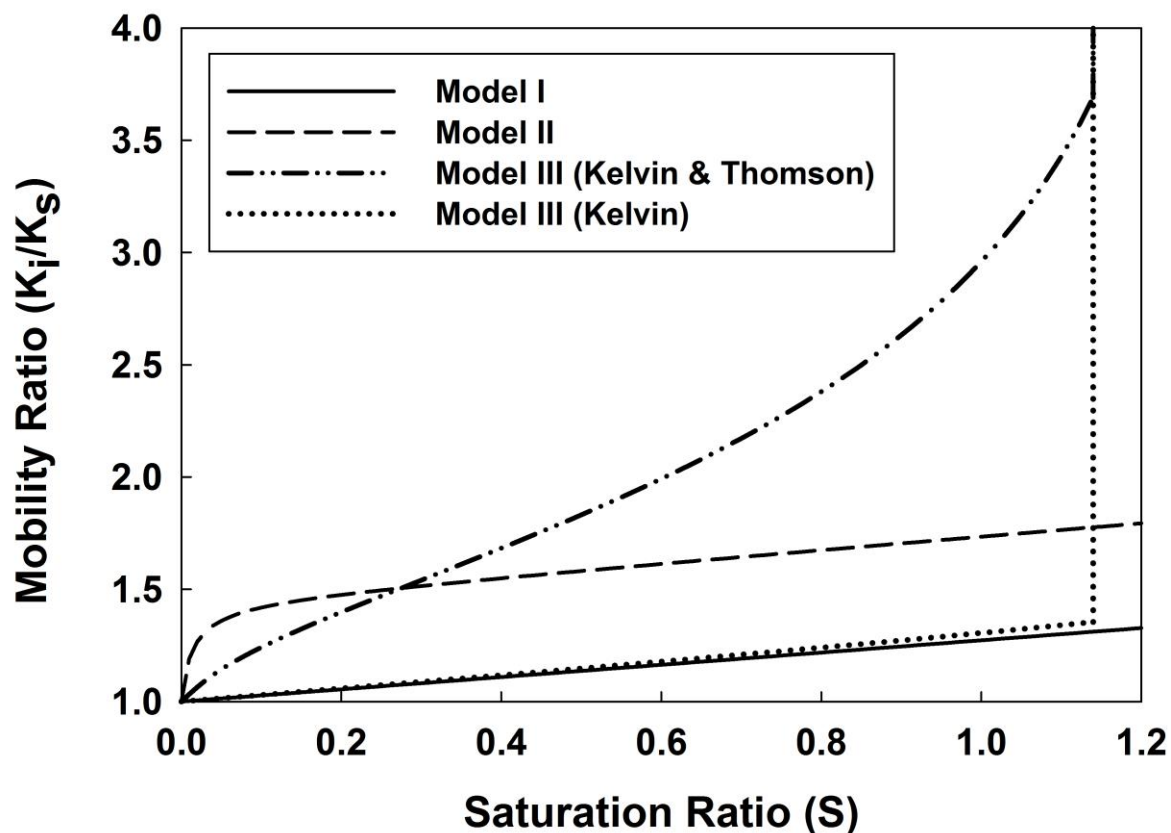


Figure 5. A comparison of the predicted mobility ratio (K_i/K_S) as a function of saturation ratio for angiotensin II with isopropanol as the vapor dopant for the three presented models. Model III predictions are plotted both including and excluding the Thomson effect (the influence of charge).

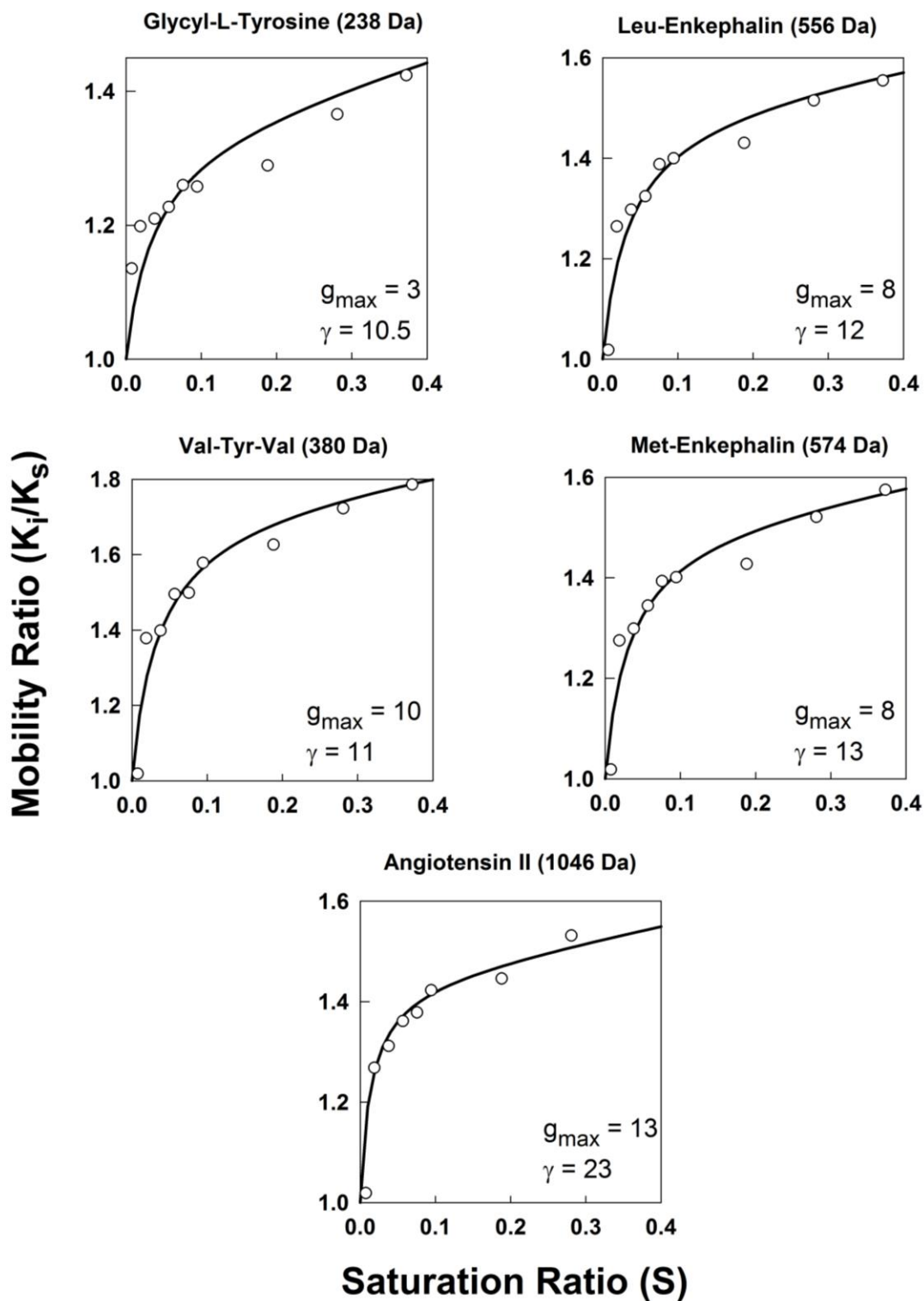


Figure 6. A comparison of experimental measurements of the ratio (K_i/K_s) for five peptide ions to model II predictions, using fit values of γ and g_{max} .

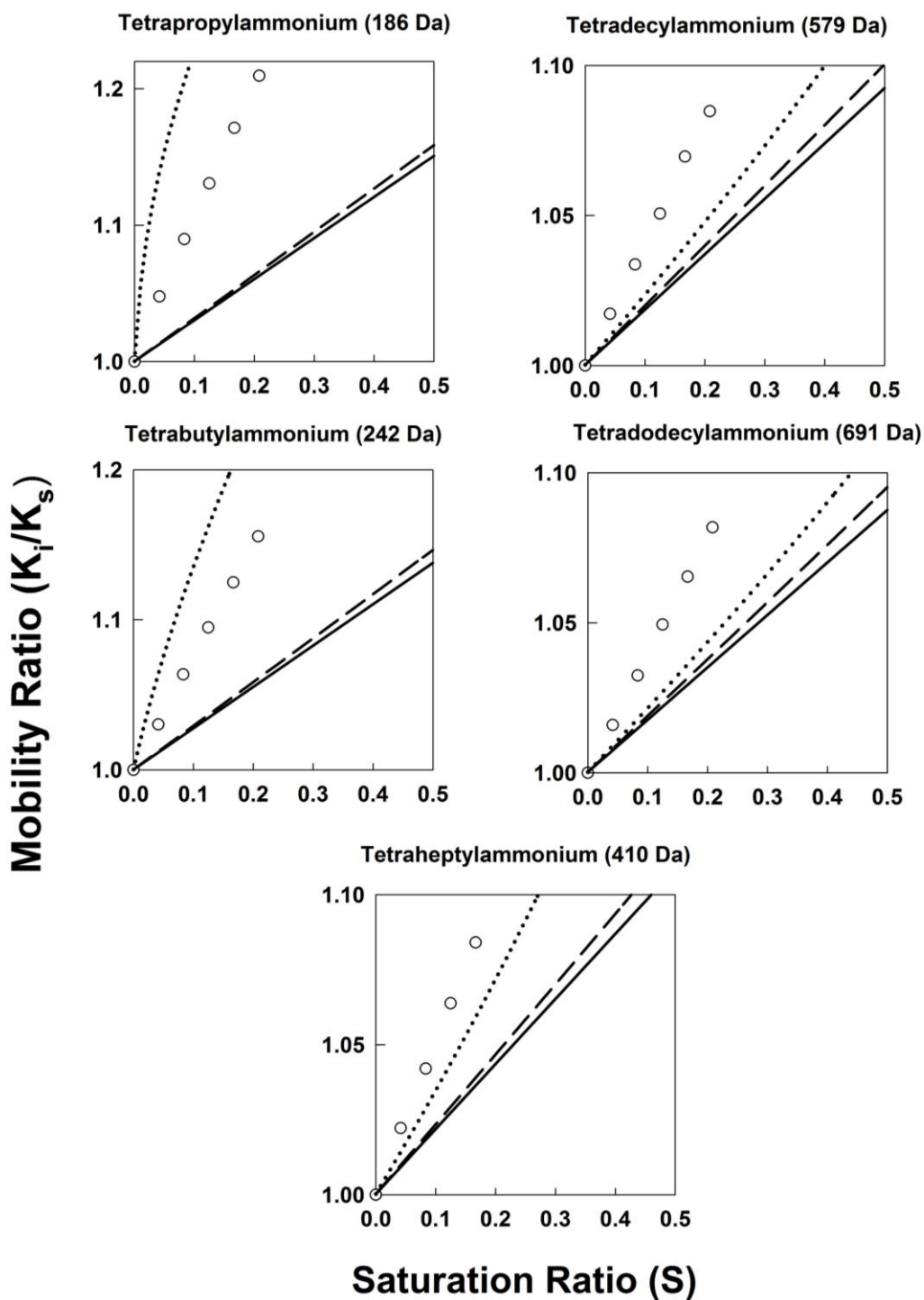


Figure 7. A comparison of experimental measurements of the ratio (K_i/K_s) for tetraalkylammonium ions to model I predictions (solid lines), model III predictions excluding the Thomson effect (long dash lines), and model III predictions including the Thomson effect (dotted lines).